Proc. Indian Acad. Sci. (Chem. Sci.), Vol. 92, Numbers 4 & 5, August & October 1983, pp. 359–377.

Extinction correction and synchrotron radiation

P SUORTTI

Department of Physics, University of Helsinki, Siltavuorenpenger 20D, SF-00170 Helsinki 17, Finland
Present address: NSLS, Brookhaven, National Laboratory Upton, New York 11973, USA

Abstract. The primary extinction factor y_p is defined as the ratio of the integrated reflection from a coherently diffracting domain to the integrated kinematical reflection from the same domain. When y_p is larger than 0·5 it may be approximated by $y_p = \exp\{-(\alpha\delta)^2\}$, where α is about 0·5 and δ the average size of the coherent domain when measured in units of the extinction length Λ, $\delta = D/\Lambda$.

Transfer equations are applied to symmetrical Laue diffraction, and the reflectivity per unit length, $\sigma(\varepsilon)$ is solved from the measured reflecting ratio as a function of the rocking angle $\varepsilon = \theta - \theta_B$.

Measurements with conventional x-ray sources are made on single crystal slabs of Be and Si using AgKβ, MoKα_1 and CuKα radiation. The primary extinction factor $y_p(\varepsilon)$ is solved from a point-by-point comparison of two measurements where the extinction length Λ is changed by varying the polarization and/or wavelength of the x-ray beam. The results show that primary and secondary extinction are strongly correlated, and that the customary assumption of independent size and orientation distributions of crystal mosaics is unjustified. The structure factors for Be and Si show close agreement with other recent measurements and calculations.

The limitations of the method are discussed in length, particularly the effects of beam divergences and incoherence of the rays in the crystal. It is concluded that under typical experimental conditions the requirements of the theory are met. Practical limitations arising from the use of characteristic wavelengths and unpolarized radiation prohibit the use of the full potential of the method.

The properties of a synchrotron radiation source are compared with a conventional x-ray source, and it is demonstrated that the experimental limitations can be removed by the use of synchrotron radiation. A diffraction experiment with synchrotron radiation is outlined, as well as generalization of the method to small spherical crystals.

Keywords. Extinction; synchrotron radiation.

1. Introduction

In his paper "The reflection of x-rays from imperfect crystals" Darwin (1922) writes about the theory of extinction which he is going to introduce: "I am afraid I have not succeeded in welding the parts of the argument rigorously together, but in spite of certain gaps in the theory it seems unlikely that there is serious error in the general views to which it leads". After more than 60 years, our understanding of extinction is still based on Darwin's views, on the concepts of primary and secondary extinction. In the main line of crystallography, correction schemes have been incorporated in procedures for structure determination, but in a sense this has been a step backwards, as the extinction calculations are based on the energy transfer equations, which cover secondary extinction only (Hamilton 1957; Zachariasen 1967; Cooper and Rouse 1970; Coppens and Hamilton 1970; Becker and Coppens 1974a, b, 1975). Moreover, the extinction corrections are derived by least squares fitting to a crystal model which includes theoretical structure factors and extinction parameters. These are highly correlated, and although the extinction correction greatly improves the average quality of the diffraction data it may also introduce artefacts.

Darwin's paper was purported to provide understanding of the experimental results by Bragg *et al* (1921, abbreviated hereafter as BJB). Since those days, there has always been a line of direct experimental approach to the problem of extinction. The kinematical limit, where the feedback between the direct and reflected beams can be ignored, has been approached in various ways. These include methods where the active volume of the crystal or the reflectivity per unit volume are reduced (for references, see Mathieson 1979).

Some of the basic ideas of the present work can be found already in Darwin's paper where he writes: "The methods used in BJB remove the secondary extinction, but are without influence on the primary. In fact, it will appear that no experiments of the present type can possibly remove it; indeed, to do so would require the measurement of the actual sizes of the small blocks of perfect crystal." . . . "Now, at each instant of the rotation there will be a different amount reflected and therefore a different extinction, and consequently it will not suffice to treat of the mean effect of extinction, without first determining it at every setting of the crystal." In the following we will see that the degrees of both primary and secondary extinctions are correlated to the reflection profile and each other, and that when the actual sizes of the coherent domains are expressed in units of extinction length the sizes can be determined from two measurements and the effects of primary extinction removed.

The details of the method have been described earlier (Suortti 1982a, b), and the aim of this paper is to outline the method, give some new results, discuss the limitations of the theory and those of an experiment with a conventional x-ray source, and finally describe how the full potential of the method is utilized by the use of synchrotron radiation.

2. Transfer equations

In the following we will assume that the radiation from the x-ray source is incoherent. For a conventional x-ray tube this is obvious, and even with a synchrotron radiation source the possible effects of wave coherence are small. Consider the two waves in figure 1, which illustrates crystal domains with constant but independent lattice phases G. When wave (1) enters domain (a) at an angle θ, which is close enough to a Bragg angle $\theta_B = \theta - \varepsilon$, two waves of electric displacements D_d and D_g are excited, and these have a constant phase difference within (a), *i.e.* the amplitudes of the waves are coupled. The resulting decrease of D_g is called primary extinction. On the other hand, the difference between G_a and G_b is arbitrary, the intensities from (a) and (b) add up. However, domain (b) is screened by diffraction in (a), in addition to the normal absorption, and this loss due to intensity coupling is called secondary extinction. Also the second diffraction of D_g in domain (c) decreases the reflected power P_g^*. The flow of energy between P_d^* and P_g^* is covered by the energy transfer equations,

$$\partial P_d^*/\partial s_d = -\mu_e^i P_d^* + \sigma_{-g} P_g^*, \tag{1a}$$

$$\partial P_g^*/\partial s_g = -\mu_e^i P_g^* + \sigma_g P_d^*, \tag{1b}$$

where (s_d, s_g) are oblique coordinates along the direct and diffracted beams, respectively. If we assume a non-polar crystal, $\sigma_g = \sigma_{-g}$, and ignore the possibility of the Borrmann effect,

$$\mu_e^i = \mu_0 + \sigma, \tag{2}$$

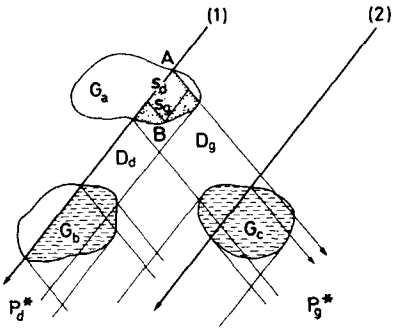

Figure 1. Diffraction from coherent domains. Within each domain, the lattice phase G is constant, but the differences between G_a, G_b and G_c are arbitrary. D_d and D_g are the electric displacements of the direct and reflected beams excited in domain (*a*). The area of coherent coupling for the ray entering (*a*) at A and exiting at B is indicated by s_d and s_g, and the total area of wave coherence with dots. The shaded areas of (*b*) and (*c*) show incoherent coupling of the direct and reflected beams of rays (1) and (2).

where $\sigma = \sigma(\varepsilon, s_d, s_g)$ is the reflectivity per unit length of the traversed crystalline medium and μ_0 the linear absorption coefficient. The observable reflectivity $\sigma(\varepsilon)$ is the integral of $\sigma(\varepsilon, s_d, s_g)$ over the region of interaction for the extended incident beam, and the integrated intensity is found by an angular integration.

3. Primary extinction

The transfer equations for two waves that have amplitude coupling were introduced by Takagi (1962, 1969) and Taupin (1964):

$$\partial D_d/\partial s_d = i\kappa_{-g} D_g \exp\{iG(s_d, s_g)\}, \tag{3a}$$

$$\partial D_g/\partial s_g = i\kappa_g D_d \exp\{-iG(s_d, s_g)\}, \tag{3b}$$

where the coupling coefficient is

$$\kappa_g = r_e \lambda C F_g / V_c. \tag{3c}$$

Here C is the polarization factor ($\cos 2\theta$ when the electric vector is in the plane of diffraction, 1 when perpendicular to that), λ the x-ray wavelength, $r_e = e^2/mc^2$ the electron scattering length, V_c the unit-cell volume, and F_g the structure factor. The lattice phase $G = 2\pi \mathbf{g} \cdot \mathbf{u}$, where $\mathbf{g}$ is the scattering vector and $\mathbf{u}$ the lattice distortion.

The two waves D_d and D_g stay coherent within the domain where G is constant. As seen in figure 1, the maximum area of coherent coupling is $s_d s_g \sin 2\theta$, and the appropriate average is found by an integration over the exit surface. The "size" of the coherent domain may be defined as the average

$$D = \overline{(s_d s_g)}^{\frac{1}{2}}. \tag{4}$$

Explicit calculation is possible for a given cross-section of a perfect crystal, and detailed results are available for square and circular shapes (Olekhnovich and Olekhnovich 1978, 1980). If the incoming ray is taken as a plane wave, reflectivity curves $R(\varepsilon)$ can be calculated; an example is illustrated in figure 2. The detailed form of $R(\varepsilon)$

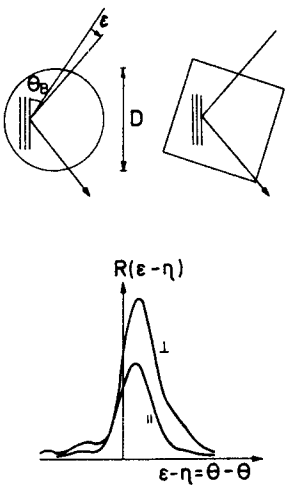

Figure 2. Regularly shaped coherent domains of size D, and typical reflectivity curves of a domain for perpendicular and parallel polarizations of the incident plane wave.

depends on the crystal shape, wavelength and polarization, but the integral of $R(\varepsilon)$ is well defined by $\kappa_g D$, and this is the basis of the extinction correction to be introduced in the following.

The integrated reflectivity due to domains of size D is (Suortti 1982a)

$$\sigma_D(\varepsilon) = \int R_D(\varepsilon - \eta) w_D(\varepsilon) \mathrm{d}\varepsilon$$

$$\simeq w_D(\varepsilon) \int_{\Delta\varepsilon} R_D(\varepsilon - \eta) \mathrm{d}\varepsilon = Q y_p(D) w_D(\varepsilon). \tag{5}$$

Here η is the deviation of domains from the average orientation, $w_D(\varepsilon)$ is the distribution function of domain sizes (which is supposed to be slowly varying in comparison with R_D), $Q = (\lambda/\sin 2\theta_B)|\kappa_g|^2$ is the integrated kinematical reflectivity per unit length (or integrated reflecting power per unit volume; see James 1962), and $y_p(D) < 1$ is the primary extinction factor. The observable reflectivity is

$$\overline{\sigma(\varepsilon)} = Q \int y_p(D) w_D(\varepsilon) \mathrm{d}D. \tag{6}$$

The integrated reflectivity per unit length of the crystallite, $Q' = Q y_p(D)$, can be expressed in terms of low-order Bessel functions J_{2n}. The argument of the functions is

$$\delta = \kappa_g H \overline{(s_d s_g)}^{\frac{1}{2}} = D/\Lambda, \tag{7}$$

where $\Lambda = (\kappa_g H)^{-1} = V_c/(r_e \lambda C F_g H)$ is the extinction length. Here H is the long-range order parameter, which for a perfect crystal is the Debye-Waller factor $\exp(-M)$. The above means that the arguments of the intensity expressions become linear in the size of the coherent domain, when this is measured in the units of Λ. The *effective size* δ can be varied by changing λ, C or F_g, and this gives an experimental possibility for

determination of primary extinction.

At small enough values of δ it follows from the properties of J_{2n} that

$$y_p(\delta) = Q'/Q = Q^{-1} \int R_\delta(\psi)\mathrm{d}\psi \simeq \exp\{-(\alpha\delta)^2\}, \tag{8}$$

where the numerical value of α is about 0·5. Model calculations (Olekhnovich and Olekhnovich 1978, 1980) suggest that this approximation is valid when $\delta < 1{\cdot}5$ or $y_p > 0{\cdot}5$. It is worth noting that the same functional form can be recovered from Darwin's (1922) original work,

$$y_p(D) = \frac{\tanh mq}{mq} \simeq \exp\{-(D/\sqrt{3}\Lambda \sin\theta)^2\}. \tag{8'}$$

the extra angular factor $(\sin\theta)^{-1}$ arises from the special geometry of a laterally infinite plate.

The primary extinction factor at a given average angle of incidence is weighted by the distribution of domain sizes,

$$y_p(\varepsilon)w(\varepsilon) = \int y_p(\delta)w\{\delta(\varepsilon)\}\mathrm{d}\delta = Q^{-1}\overline{\sigma(\varepsilon)}. \tag{9}$$

If we assume that $w\{\delta(\varepsilon)\}$ is a Gaussian of width $2\Delta_\varepsilon$, centred at $\overline{\delta_\varepsilon}$, convolution resulting from substitution of (8) to (9) yields

$$y_p(\varepsilon) = \exp\{-(\alpha\overline{\delta_\varepsilon})^2/(1+\alpha\sqrt{2}\Delta_\varepsilon)^2\} = \exp\{-(\alpha'\overline{\delta_\varepsilon})^2\}. \tag{10}$$

Although idealized, this calculation suggests that the functional form of (8) can be used also for real crystals.

The primary extinction factor can be determined from two measurements of $\overline{\sigma}(\varepsilon)$ where the extinction length is changed. Writing δ_1 and δ_2 for $\overline{\delta_\varepsilon}$ in (10) and assuming that the effective crystal volume is the same in both measurements, one obtains from (10)

$$f(\varepsilon) = \frac{y_{p,1}(\varepsilon)}{y_{p,2}(\varepsilon)} = \exp\{-(\alpha'\delta_1)^2(1-(\delta_2/\delta_1)^2)\}$$

$$= \frac{Q_2}{Q_1} \cdot \frac{\sigma_1(\varepsilon)}{\sigma_2(\varepsilon)}. \tag{11a}$$

The correction for primary extinction in measurement 1 is

$$y_{p,1}(\varepsilon) = \{f(\varepsilon)\}^\beta, \tag{11b}$$

where

$$\beta^{-1} = 1-(\Lambda_1/\Lambda_2)^2. \tag{11c}$$

The extinction length Λ can be varied by changing the polarization factor C or the wavelength λ. A change in λ usually entails a change of C, and

$$\beta_\lambda^{-1} = 1-(\lambda_2 C_2/\lambda_1 C_1)^2. \tag{12a}$$

If the polarization of the beam is parallel to the plane of diffraction in one measurement, $C_1 = |\cos 2\theta|$, and perpendicular to this plane in the other, $C_2 = 1$,

$$\beta_C^{-1} = 1-\sec^2 2\theta. \tag{12b}$$

4. Secondary extinction

The energy transfer equations must be solved under the boundary conditions. A simple closed-form solution is available only for a parallel-sided crystal, but an iterative solution can be presumably found for any simple polyhedral crystal, when the so-called *AB*-extinction formulas by Werner (1974) are used. The quantity determined experimentally is called the reflecting ratio

$$r^*(\varepsilon) = \frac{P_g^*(\varepsilon)}{AP_{d,o}}, \tag{13}$$

where A is the absorption factor, and $P_{d,o}$ the incident beam. In the situation illustrated in figure 3, where the crystal is bathed in the incident beam, determination of $AP_{d,o}$ may require extensive subsidiary measurements. The corrected reflecting ratio, where the decrease of P_d due to diffraction is counted for, is defined by

$$r^*(\varepsilon) = y_s(\varepsilon) r(\varepsilon), \tag{14a}$$

where $y_s(\varepsilon)$ is the secondary extinction factor. From conservation of energy, which is demonstrated in the figure,

$$r(\varepsilon) = \frac{r^*(\varepsilon)}{1 - r^*(\varepsilon)}. \tag{14b}$$

The boundary conditions come into the play when the reflectivity $\sigma(\varepsilon)$ is to be solved from $r(\varepsilon)$.

Laue diffraction from a parallel-sided crystal plate is illustrated in figure 4, and the powers of the reflected and direct beams can be written as

$$P_g^*(\varepsilon) = P_{d,o} \exp(-aT) \sinh(\sqrt{a^2 - b}\, T), \tag{15a}$$

$$P_d^*(\varepsilon) = P_{d,o} \exp(-aT)\{(\gamma_g/\sigma)\sqrt{a^2 - b}\, \cosh(\sqrt{a^2 - b}\, T) + ((\mu_0 + \sigma)/2\sigma)(1 - \gamma_g/\gamma_d) \cdot \sinh(\sqrt{a^2 - b}\, T). \tag{15b}$$

The geometrical factors are explained in the legend of figure 4, and

$$a = \tfrac{1}{2}(\mu_0 + \sigma)(1/\gamma_g + 1/\gamma_d), \tag{15c}$$

$$b = (\mu_o^2 + 2\mu_o\sigma)/(\gamma_g\gamma_d). \tag{15d}$$

The absorption factor for the transmitted beam is $A = \exp(-\mu_o T/\gamma_d)$, and the observed

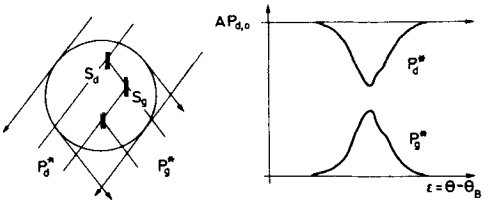

Figure 3. Crystal bathed in the incident beam. P_d^* is the measured power of the direct beam and P_g^* that of the reflected beam, and $AP_{d,0}$ is the transmitted beam when there is no diffraction. By conservation of energy, $P_g^* + P_d^* = AP_{d,0}$.

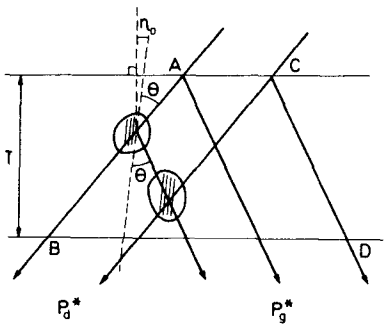

Figure 4. Laue diffraction from a parallel-sided crystal plate. The incident beam extends from A to C, the reflected from B to D. The average orientation of reflecting domains deviates from the plate normal by η_0, and following notations are used $\gamma_d = \cos(\theta + \eta_0)$, $\gamma_g = \cos(\theta - \eta_0)$.

reflecting ratio

$$r^*(\varepsilon) = \exp\{-\tfrac{1}{2}\mu_o T(1/\gamma_d - 1/\gamma_g) \times \exp\{-\tfrac{1}{2}\sigma T(1/\gamma_d + 1/\gamma_g)\} \cdot \sinh(\sqrt{a^2 - b}\, T). \tag{16}$$

The reflectivity per unit length, $\sigma(\varepsilon)$, can be solved from the experimental $r^*(\varepsilon)$. The formulas become cumbersome, except in the symmetrical case where $\gamma_g = \gamma_d = \cos\theta$, and with (14),

$$r(\varepsilon) = \sinh(\sigma T/\cos\theta) \simeq \sigma(\varepsilon)T/\cos\theta. \tag{17}$$

Small deviations from symmetry can be considered as miscut of the crystal, and corrected for by using series expansions of (15).

5. Experimental results

The method realizes Darwin's appeal that extinction is to be determined at each setting ε of the crystal. This imposes stringent bounds to the experimental situation: on the one hand, the divergences should not smear $r^*(\varepsilon)$ or $\sigma(\varepsilon)$, on the other, $y_p(D)$ is determined only by integration over $R_D(\varepsilon - \eta)$. Therefore, it is advisable to estimate $\Delta\varepsilon$ in (5) and compare it with typical widths of reflections.

We are interested in the cases where $y_p(\delta) < 0{\cdot}99$, or $\delta > 0{\cdot}2$; for smaller coherent domains the integral over $R_D(\varepsilon - \eta)$ is always Q. The total width of R_D is approximately $2\lambda/D$, and at the above limit $\Delta\varepsilon \simeq 10\lambda/\Lambda$. Table 1 gives a few typical values for the strongest reflections of various crystals, and the results indicate that $\Delta\varepsilon$ is of the order of 0·1 mrad for light materials.

The upper limit for the divergence is due to the requirement that $r^*(\varepsilon)$ should not be appreciably smeared by $\Delta\varepsilon$. The possible minimum width of a reflection can be estimated as follows: at the kinematical limit $Q = \sigma_{\text{kin}}(0)\beta$, where β is the integral width of the reflection, and in the present geometry, $\sigma_{\text{kin}} = r_{\text{kin}}/(T/\cos\theta)$. The maximum value of $r_{\text{kin}}(0)$ is 1, which corresponds to $r^*(0) = 0{\cdot}5$, and so $\beta_{\min} = QT/\cos\theta$. For instance, $\beta_{\min}$ for Be(00·2) measured with MoKα from a 1·1 mm thick crystal is 0·35 mrad, and

Table 1. Extinction lengths (in units of μm) and widths of reflectivity curves (in units of mrad) of domains with $D/\Lambda = 0{\cdot}2$ for the strongest reflections of various crystals at a few x-ray wavelengths λ.

	$\lambda = 0{\cdot}561$ Å		$\lambda = 0{\cdot}710$ Å		$\lambda = 1{\cdot}542$ Å	
Refl.	Λ	$\Delta\varepsilon$	Λ	$\Delta\varepsilon$	Λ	$\Delta\varepsilon$
Be(00·2)	30·5	0·02	24·1	0·03	11·1	0·14
LiF(200)	14·0	0·04	11·0	0·06	5·1	0·30
Al(111)	12·2	0·05	9·7	0·07	4·5	0·34
Si(220)	14·9	0·04	11·8	0·06	5·4	0·29
Fe(110)	4·1	0·14	3·2	0·22	1·5	1·03

for Si(220) of the same thickness 1·5 mrad; these values are an order of magnitude larger than $\Delta\varepsilon$ in table 1.

The above considerations determined the experimental arrangement, which has been explained in detail earlier (Suortti 1982b). In the case of Be, the non-dispersive (1, −1) arrangement of the monochromator and sample crystal could be used, and in the case of Si, $K\alpha_2$ component of radiation could be eliminated by narrow collimation. The measuring geometry is illustrated in figure 5. $MoK\alpha_1$ and $AgK\beta$ were obtained by reflection from a Si(220) flat monochromator, which had a rocking curve width of 0·1 mrad. $CuK\alpha$ was selected by a polarizer-monochromator which was based on anomalous transmission or Borrmann effect. The electric vector of the transmitted beam lies in the diffracting planes and can be rotated by rotating the Ge(220) Borrmann crystal about the axis of the x-ray beam.

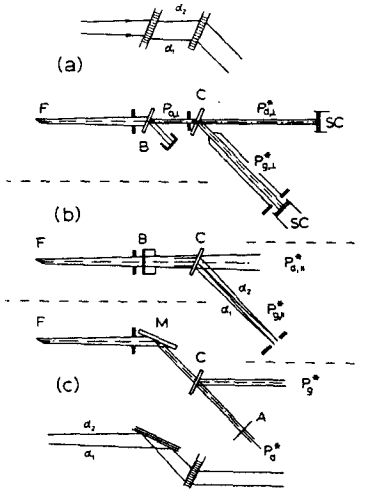

Figure 5. Measuring geometry in the plane of diffraction with a Borrmann polarizer B (**a** and **b**) and reflecting monochromator M (**c**). The point focus of the x-ray tube is indicated by F, the sample by C, and the scintillation counter by SC. The forward diffracted beam from the polarizer is used, and the other beam is caught by a beam stop shown in (**a**). The inserts in (**a**) and (**c**) show the non-dispersive setting when the Bragg angle of the polarizer or monochromator is equal to that of the sample crystal.

The measurement on Be was made with (almost) unpolarised MoKα_1 and with polarized CuKα. Si was measured with AgKβ and MoKα_1. The reflections were step-scanned in intervals of 0·05 to 0·1 mrad, and the power of the primary beam was measured by the same scintillation detector. With MoKα_1 and AgKβ an accurately calibrated attenuator was needed. The reflecting ratio $r(\varepsilon)$, which is corrected for secondary extinction, was calculated at each angle of measurement, and $y_p(\varepsilon)$ was determined from comparison of two measurements of the same reflection when the extinction length Λ was varied through λ or C. The details of this procedure have been given earlier (Suortti 1982b).

Some of the results are reproduced in table 2 together with earlier experimental and theoretical values, and plots of a few reflections are shown in figure 6. The structure factors of Be are based on quite a few measurements at different locations of the crystal, and the agreement with other recent values is very good, although the average primary and secondary extinction corrections reach 30 %, and the peak values of $y_s^{-1} - 1$ and $y_p^{-1} - 1$ are much larger. The implications of the results have been discussed in detail by Larsen and Hansen (1983), who conclude that the charge density distribution in Be metal can be interpreted by sp^3 hybridization, where the orbitals are directed towards the tetrahedral holes. The situation is well described by an LCAO calculation (Dovesi *et al* 1982), although some of the features are exaggerated. The measurement on Si is a real test case of the method, as the true values of $F(hkl)$ for MoKα radiation are known very accurately from the Pendellösung measurements by Aldred and Hart (1973). Considering that the experimental situation was quite unfavourable, as the crystal was too thick and so the extinction corrections always large, the results are very satisfactory and substantiate the soundness of the method.

It is worth noting that the degree of primary extinction, $y_p^{-1}(\varepsilon) - 1$, follows closely the reflectivity curve when the reflection is narrow, while $y_p(\varepsilon)$ of a wide reflection is almost constant. The former behaviour is not covered by the customary version of the

Table 2. Experimental and theoretical structure factors of Be and Si at room temperature.

Be:				
hk·l	Present	HSL	LH	DPRR
10·0	1·90 ± 0·01	1·83	1·85	1·914
00·2	3·37 ± 0·02	3·32	3·37	3·397
10·1	2·78 ± 0·03	2·83	2·84	2·810

Si:		
hkl	Present	AH
111	59·60	60·55
220	69·10	67·84
113	44·90	43·96
222	1.48	1.35 (calc.), 1.50 (ref.)
004	56·70	56·62

The entries for Be include a measurement with γ-rays (Hansen *et al* 1983), a conventional measurement from a small crystal with AgKα and MoKα radiations (Larsen and Hansen 1983), and results of an LCAO calculation (Dovesi *et al* 1982). The theoretical values have been multiplied by the Debye-Waller factor $\exp(-B \sin^2\theta/\lambda^2)$, where $B_{11} = 0{\cdot}460\ \text{Å}^2$ (in basal plane) and $B_{33} = 0{\cdot}415\ \text{Å}^2$ (perpendicular to basal plane). The reference values for Si are from a Pendellösung measurement by Aldred and Hart 1973.

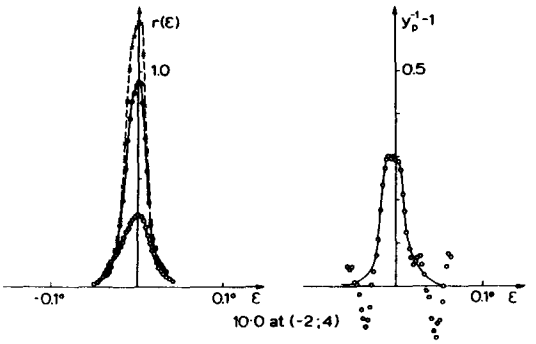

Figure 6a. Reflecting ratio $r(\varepsilon)$ and the corresponding correction for primary extinction as a function of the rocking angle $\varepsilon = \theta - \theta_B$ of the Be crystal. Open circles (○) give $r(\varepsilon) = r_2(\varepsilon)$ with CuKα radiation, and the results with MoKα are brought to the same scale by multiplying by $(Q_2/Q_1)(\cos\theta_1/\cos\theta_2)$; filled circles (●) indicate $r(\varepsilon) = r_1(\varepsilon)$ before and crosses (×) after the correction for primary extinction.

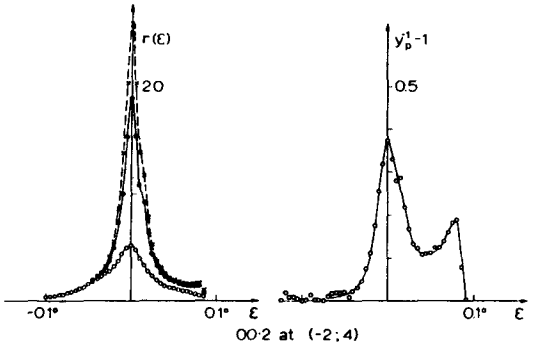

Figure 6b. See the legend of figure 6a.

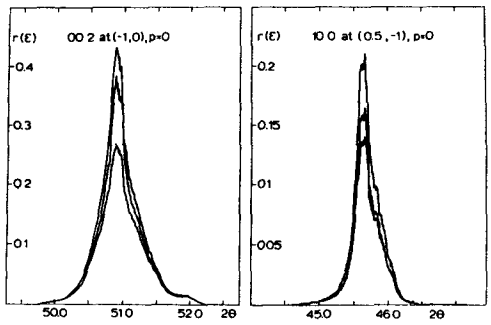

Figure 6c. Reflecting ratio of the measurements with polarized CuKα radiation. The lowest curve is the measured profile $r^*(\varepsilon)$ when $C = 1$, the middle one, $r(\varepsilon)$, is corrected for secondary extinction, and the top curve is the kinematical reflection profile calculated from the comparison with the measurement with $C = |\cos 2\theta|$. The scale is the same as in figure 6a.

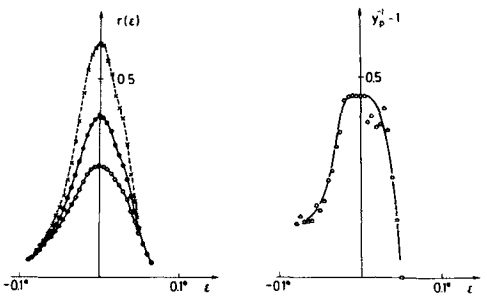

Figure 6d. Reflecting ratios for Si(111) measured with unpolarized AgKβ (filled circles, ●) and MoKα_1 (open circles, ○). For details, see the legend of figure 6a.

mosaic-crystal model, where the orientation and size distributions are independent. This implies a constant primary extinction over the profile, and the rest of the effect is termed secondary extinction, which is either orientation-determined (type I) or size-determined (type II) according to Zachariasen (1967) (see the next section). The present results show, however, that $y_p(\varepsilon)$ and $y_s(\varepsilon)$ are often strongly correlated, and that interpretations based on the mosaic-crystal model may lead to false conclusions (*cf.* Olekhnovich *et al* 1980).

6. Limitations of the method

Questions of validity concern the underlying principles as well as the practical realization of the method. Some of the problems have been discussed in detail in earlier papers (Suortti 1982a, b), and will be only mentioned here.

6.1 *Divergences of the beams*

The central question is that of the divergences of the beams inside the crystal. In Darwin's words: ". . . each layer will, on account of diffraction, spread out incident parallel rays into a certain range of angles and so will continually change the angle at which they attack the successive layers". In practice, the incident beam has certain divergences, and figure 7 illustrates how the divergences develop in diffraction by coherent domains. The divergence $\Delta\varepsilon$ is taken to be large enough to cover $R_\delta(\varepsilon)$ when $y_p < 0{\cdot}99$. The largest domain reflects only a narrow band of the available rays, and its contribution to the reflectivity is $\sigma_1(\varepsilon, \varepsilon + \Delta\varepsilon) = Qy_{p,1}$; in this case the divergence of the direct beam is retained, and the g-beam has less divergence. This is convoluted, however, by the orientation distribution of the domains, and the divergence of the macroscopic g-beam roughly equals to that of the d-beam. The second domain has a reflectivity curve which fits the divergence $\Delta\varepsilon$, and so d- and g-beams have equal divergences. For this domain already $\sigma(\varepsilon, \varepsilon + \Delta\varepsilon) \simeq Q$. The third, very small domain spreads out the g-beam, and the successive reflections make the same happen to the d-beam.

From the above discussion it is clear that when the domains are large enough to exhibit primary extinction the divergence of the incident beam can be selected such that it is retained in the successive reflections. In that case the energy transfer equations (1)

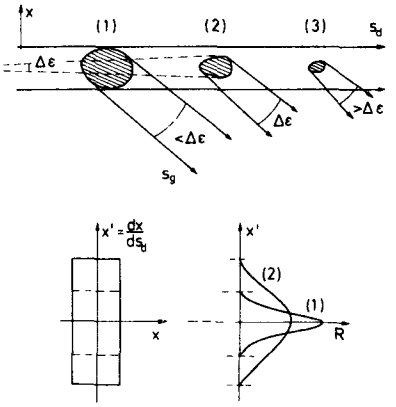

Figure 7. Reflection of a beam with divergence $\Delta\varepsilon$ from coherent domains of variable size. In the lower part, the width x and divergence $x'(=\varepsilon)$ of the beam are illustrated as a phase-space diagram together with the reflectivity curves of domains (1) and (2).

apply, and the effects of primary extinction on $\bar{\sigma}(\varepsilon)$ are covered by $y_p(\varepsilon)$.

If the effects of primary extinction are negligible,

$$\int R_\delta(\varepsilon-\eta)\mathrm{d}\varepsilon = Q \tag{18}$$

for all δ. The average kinematical reflectivity for the extended beam becomes

$$\sigma_{\mathrm{kin}}(\varepsilon) = \int\int R_\delta(\varepsilon-\eta)w_\delta(\varepsilon)\mathrm{d}\eta\,\mathrm{d}\delta = \int R(\varepsilon-\eta)w(\eta)\mathrm{d}\eta, \tag{19}$$

where $R(\varepsilon-\eta)$ is the average reflectivity of the domains oriented in an angle η, and $w(\eta)$ is the normalized abundance of these domains. In his theory of secondary extinction, Zachariasen (1967) distinguishes two cases on the basis of the wider, dominant distribution,

$$\sigma_{\mathrm{kin}}(\varepsilon) = Qw(\varepsilon), \quad \text{type I}, \tag{20a}$$

$$\sigma_{\mathrm{kin}}(\varepsilon) = R(\varepsilon), \quad \text{type II}. \tag{20b}$$

Figure 8 illustrates the effects of diffraction on the divergences in the two cases. In the type-I crystal the beams are not substantially spread, but in a type-II crystal the divergences of the beams cover the whole reflecting range already after a few reflections inside the crystal. For a type-I crystal the preceding formalism applies, and it can be shown that the correction for secondary extinction would be correct to the first order also for a type-II crystal.

As pointed out by Kato (1980a), the problems arising from the convolution of scan and divergences can be avoided when the incident beam is a spherical wave. A first-order correction for secondary extinction would still be possible, but in a correction for primary extinction a constant y_p should be assumed.

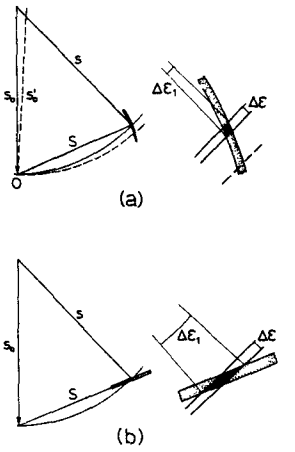

Figure 8. Ewald construction for diffraction from a type-I crystal (**a**) and a type-II crystal (**b**). The broken lines in (**a**) show the effect of variation of the incident beam direction. The inserts illustrate the active volume of the diffraction domain, when $\Delta\varepsilon$ is the divergence of the incident beam.

6.2 *Incoherence of the beams*

The basic idea of the method is that the d- and g-beams experience a sufficient number of reflections as to lose mutual coherence. In the terminology introduced by Kato (1980b), a ray entering the crystal leaves the coherent channel. The number of reflections experienced by a narrow ray can be estimated from figure 4. The approximation (8) is valid only when $\delta < 1{\cdot}5$ or when the domains are smaller than $3\Lambda/2$. In the symmetrical Laue geometry, the area of interaction for each ray is $2T^2 \tan\theta$, and so there are about $(T/\Lambda)^2 \tan\theta$ domains of the maximum size in this area. Simultaneously reflecting is only the fraction $\Delta\varepsilon/\beta$, and with the typical values quoted earlier, 10 to 100 domains contribute to reflection of each ray.

Although the above result suggests that the requirements of the theory are met in a typical measurement, it is worth studying what happens to a ray that stays in the coherent channel. This means that the g-beam from the first coherent domain is not re-reflected, and so the contribution to the measured reflecting ratio is $\delta r^*(\varepsilon) = \delta r(\varepsilon) = \sigma(\varepsilon, s_d, s_g')\delta T_{\text{eff}}$. This should not be corrected for the effects of secondary extinction through (14), as there are none, but only for primary extinction. Accordingly, there is the possibility of over-correction, which should be eliminated by maximizing the number of domains in the area of interaction, so that the coherent contribution to $r^*(\varepsilon)$ would be small. In general, the smaller $r^*(\varepsilon)$ the smaller is the correction for secondary extinction and also the possible error. Multiple peaks of reflections are due to diffraction from independent coherent domains, and this kind of data should be treated with special care.

The inverse problem of a crystal subject to secondary extinction only is trivial. In that case $f(\varepsilon)$ in (11a) is always unity, and therefore $y_p(\varepsilon) = 1$. However, the reflectivity curves $\sigma_1(\varepsilon)$ and $\sigma_2(\varepsilon)$ of a type-II crystal should not be compared, if these are measured with different wavelengths, because the width of $R(\varepsilon)$ is proportional to λ. In that case, only the integrals are comparable.

6.3 *Measuring geometry*

The application of the method requires that the incident beam has small divergences, which do not smear the reflection profile. In practice, $\Delta\varepsilon$ must be only about 0·1 mrad. If the crystal is rocked across the beam only in one direction, the other divergence is allowed to be much larger, and the required power of $P_0 = 10^4$ to 10^5 c/sec is easily achieved. In the measurements with polarized x-rays the plane of diffraction is rotated by 90° about the axis of the beam, and the solid angle of the incident beam should be only about 10^{-8} sr. This requirement cannot be fulfilled with a conventional source, and in the measurement quoted earlier an algorithm was developed for solution of $y_p(\varepsilon)$. This was based on assumptions of the relation between $r^*(\varepsilon)$ and $y_p(\varepsilon)$, which was deduced from measurements with two wavelengths.

Another practical limitation of the method arises from the discrete set of wavelengths that is available. The wavelengths should be optimized in regard of absorption and to make β in (11) and (12) sufficiently different from zero. In general, the use of a polarized beam should be favoured, as in this case the change in Λ does not introduce any change in the illuminated volume or other geometrical parameters, and more fundamentally: scans in reciprocal space can be made identical. However, 2θ values of the first reflections may become too small for a polarization measurement, and so λ must be varied.

7. Characteristics of synchrotron radiation

Synchrotron radiation of x-ray wavelengths (SXR) is produced in storage rings where the electron (or positron) energy is a few GeV. The spectral and angular distributions of the radiation from various elements of the ring differ greatly, and the present discussion is limited to the continuous spectrum from a bending magnet or wiggler. Figure 9 shows a universal spectral curve. Typically $B = 1{\cdot}2\,T$, $E = 2$ to 5 GeV, and so λ_c order of 1 Å. The photon flux is integrated over the vertical direction, where the SXR beam is well collimated, and a typical horizontal aperture is order of 1 mrad. The electron or

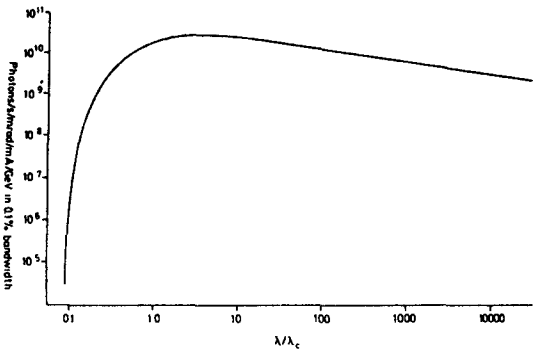

Figure 9. Universal spectral curve for synchrotron radiation from a bending magnet of an electron (positron) storage ring. The numbers correspond to unit of horizontal divergence (mrad), electron beam current (mA), and electron energy (GeV). The flux is integrated over the vertical divergence, and λ_c is the characteristic wavelength, which corresponds to the median of the power distribution.

positron current of the present-day rings is about 100 mA, and so the maximum flux to a 0·1 % bandwidth ($\Delta\lambda/\lambda = 10^{-3}$) is 10^{12} to 10^{13} photons in second. The flux on the sample depends on the actual optical solution of the beam line, and a schematic construction with focussing mirrors and a two-crystal monochromator is shown in figure 10. The insert shows a calculated intensity distribution at the sample site, and the flux is about 10^{12} photons/sec with $\Delta\lambda/\lambda = 10^{-4}$ (Hastings *et al* 1983). The flux needed for the present method is far less, but these estimates ensure that there is sufficient flux at all the wavelengths needed even with very narrow collimation and good energy resolution.

The intensity and divergence distributions of the SXR beam can be illustrated by a phase-space diagram (figure 11). Each electron under radial acceleration emits a cone of radiation, which is linearly polarized in the plane of the electron orbit and elliptically outside; the figure shows the polarization components separated. The photon opening angle depends on the electron energy and the x-ray wavelength. The parallel component has almost a Gaussian distribution with variance

$$\sigma_r = 0{\cdot}57\gamma^{-1}(\lambda/\lambda_c)^{0{\cdot}43}, \tag{21}$$

where $\gamma = E/mc^2$. Typically σ_r is order of 0·1 mrad. The beam sweeps in the horizontal plane, so the horizontal distribution is uniform, and the divergence is determined by the horizontal aperture. The electrons move in bunches, which have cross-section of order 1 mm^2, and the effective source is the convolution of the radiation and electron beam distributions, as illustrated in figure 11.

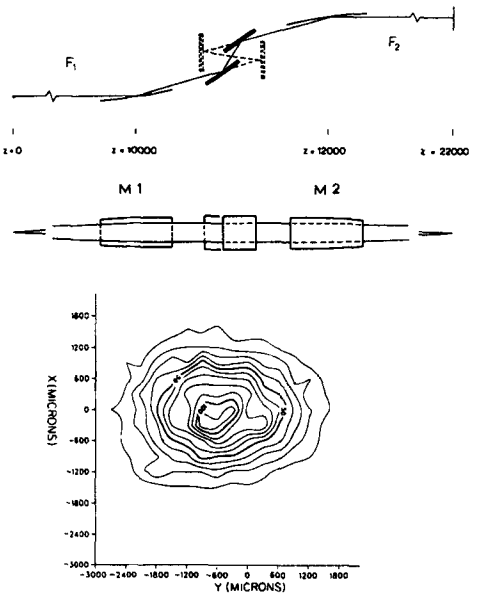

Figure 10. Schematic construction of an SXR beam line with 1 : 1 focussing. *M*1 and *M*2 are horizontally focussing grazing incidence mirrors, and the two-crystal monochromator is designed to retain the beam position. The distances *z* are in mm and typical for an x-ray beam line. The lower part shows an intensity distribution at the sample site, as obtained from a ray-tracing calculation (Hastings *et al* 1983).

The phase-space diagram propagates down the beam line. In the general case it is convoluted by the focussing functions, but figure 12 shows a simple case which does not involve any curved crystals or mirrors. In the SXR source the position and divergences are coupled, and so the intensity distributions at the sample site are non-uniform, in contrast to those from a conventional x-ray source (*cf.* figure 7). A scan by a crystal is shown in the figure. A small crystal with a very narrow reflectivity curve can be used as a probe, but in our case the sample crystal has reflection profiles that are wide in comparison with the divergence of the SXR beam. The polarization of the beam is an important parameter of the experimental situation. In a simple case, as illustrated in figure 12, the degree of polarization could be calculated from the source parameters, but generally it must be measured. The results in the figure show that perfect linear

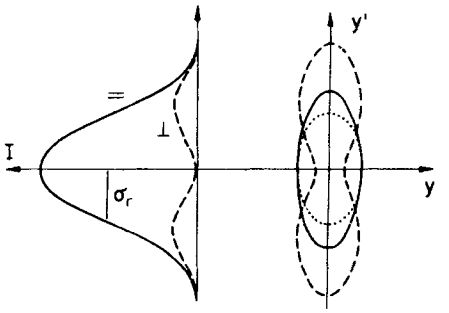

Figure 11. Components of the radiation distributions of one electron (left, = in the orbit plane, ⊥ perpendicular to the plane). Synchrotron radiation source in phase-space (right, vertical distributions). The dotted line is the 1σ-contour for the electron beam. The solid line is the contour of the parallel component, and the broken line that of the perpendicular component.

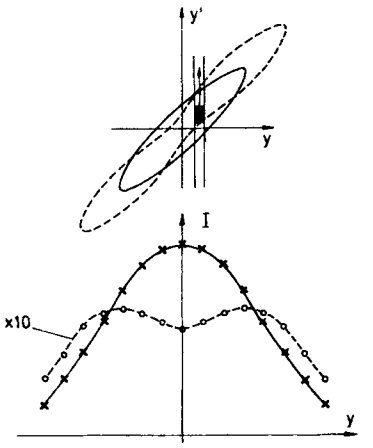

Figure 12. The phase-space diagram at distance z from the source; the figure is obtained from figure 11 by $y \rightarrow y + y'z$. The shaded rectangle shows the effective area of reflection from a small crystal, and the arrow indicates the angular scan. The lower part shows the measured average distributions of the parallel and perpendicular components across the beam.

polarization is not found even in the orbit plane unless a polarizing x-ray optical element such as a Borrmann crystal is inserted in the beam line (Materlik and Suortti 1983).

8. Outline of extinction measurement

The principle of the determination of primary extinction is illustrated in figure 13. According to (8), the primary extinction factor y_p of a coherent domain is approximately a Gaussian function of Λ^{-1}. The width of the Gaussian is inversely proportional to the size of the domain, and generally varies with the rocking angle ε of the crystal. When a conventional x-ray source is used $\Delta\varepsilon$ may be appreciable, as in the measurement with a beam polarized in the plane of diffraction, and $y_p(\varepsilon)$ varies in a non-linear fashion within $\Delta\varepsilon$. Moreover, Λ_1 and Λ_2 are determined by the available wavelengths, so that the situation cannot be optimized. These restrictions are removed by the use of SXR.

In conclusion, a practical geometrical arrangement, which is planned for the crystallography beam line of the NSLS at Brookhaven National Laboratory is depicted in figure 14. The 4-circle diffractometer is built only for a vertical scan, but an extra scan in the horizontal plane is easily adapted. The beam is monochromatized with two Si crystals in $(n, -n)$ setting, and polarized with a Borrmann crystal placed in front of the incident beam monitor. The estimated flux on 1 mm^2, when there are no focussing elements in the beam line, is 10^8 to 10^9 c/sec. This high flux makes feasible very detailed studies of the diffraction properties of crystals with a probing beam of size 10^{-2} mm^2 or less.

The method can be extended to crystals which are used customarily in crystallography. Through careful measurements of the intensity of the incident beam, $r^*(\varepsilon)$ can be determined for a crystal bathed in the beam, and the secondary extinction factor is found by (14). Kawamura and Kato (1983) have given the relation between σ, μ_0 and the radius of a spherical crystal in an easily applicable form. Their calculation is for the average σ and y_s, but it is valid also for well collimated beams, if the conditions discussed in § 6.1 are met.

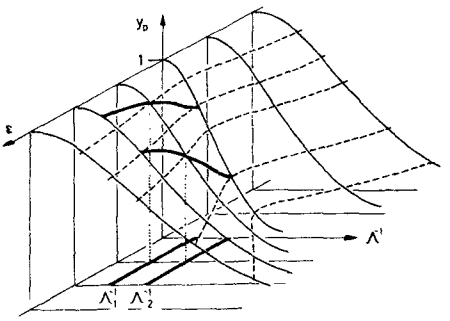

Figure 13. Primary extinction factor y_p as a function of the rocking angle ε of the crystal and the extinction length Λ. The domain size $\delta = \delta(\varepsilon)$ is largest at $\varepsilon = 0$. The divergence of the beam $\Delta\varepsilon$ makes the measurement cover a corresponding range of y_p-values (thick lines), shown for two values of Λ.

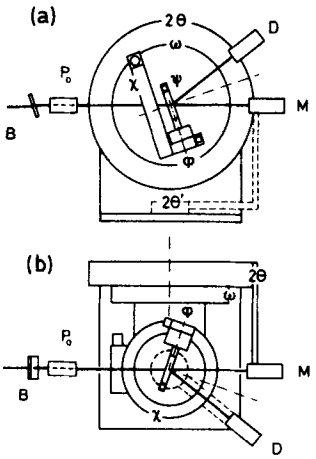

Figure 14. A modified 4-circle diffractometer at an SXR beam line: (a) vertical scan, (b) horizontal scan. B is the Borrmann polarizer, the incident power P_0 is measured by an ionization chamber. The crystal is set to the reflecting position by the χ-, ϕ-, ψ- and ω-circles, scanned by ω and 2θ in the vertical plane, or by χ and $2\theta'$ in the horizontal plane. The additions to the original construction (the ψ- and $2\theta'$-circles) are needed for a horizontal scan; $2\theta'$-circle is indicated by broken lines. D is the detector and M the monitor; the roles are interchanged in the two measurements.

Acknowledgements

The author is grateful to N K Hansen and F K Larsen for communicating their unpublished results, and to J R Schneider and A Freund for loan of the deformed Si crystal.

References

Aldred P J E and Hart M 1973 *Proc. R. Soc. London* **A332** 223
Becker P J and Coppens P 1974a *Acta Crystallogr.* **A30** 129
Becker P J and Coppens P 1974b *Acta Crystallogr.* **A30** 148
Becker P J and Coppens P 1975 *Acta Crystallogr.* **A31** 417
Bragg W L, James R W and Bosanquet C H 1921 *Philos. Mag.* **42** 1
Cooper M J and Rouse K D 1970 *Acta Crystallogr.* **A26** 214
Coppens P and Hamilton W C *Acta Crystallogr.* **A26** 71
Darwin C G 1922 *Philos. Mag.* **43** 800
Dovesi R, Pisani C, Ricca F and Roetti C 1982 *Phys. Rev.* **B25** 3731
Hamilton W C 1957 *Acta Crystallogr.* **10** 629
Hansen N K, Schneider J R and Larsen F K 1983 *Phys. Rev. B*, to be published
Hastings J B, Suortti P, Thomlinson W, Kvick A and Koetzle T F 1983 *Nucl. Instrum. Methods* **208** 55
James R W 1962 *The optical principles of the diffraction of x-rays* (London: Bell)
Kato N 1980a *Acta Crystallogr.* **A36** 171
Kato N 1980b *Acta Crystallogr.* **A36** 763
Kawamura T and Kato N 1983 *Acta Crystallogr.* **A39** 305
Larsen F K and Hansen N K 1983 Univ. Aarhus unpublished report
Materlik G and Suortti P 1983 *J. Appl. Crystallogr.* to be published

Mathieson A McL 1979 *Acta Crystallogr.* **A35** 50
Olekhnovich N M, Markovich V L and Olekhnovich A I 1980 *Acta Crystallogr.* **A36** 989
Olekhnovich N M and Olekhnovich A I 1978 *Acta Crystallogr.* **A34** 321
Olekhnovich N M and Olekhnovich A I 1980 *Acta Crystallogr.* **A36** 22
Suortti P 1982a *Acta Crystallogr.* **A38** 642
Suortti P 1982b *Acta Crystallogr.* **A38** 648
Takagi S 1962 *Acta Crystallogr.* **15** 1311
Takagi S 1969 *J. Phys. Soc. Jpn* **26** 1239
Taupin D 1964 *Bull. Soc. Fr. Minéral. Cristallogr.* **87** 469
Werner S A 1974 *J. Appl. Phys.* **45** 3246
Zachariasen W H 1967 *Acta Crystallogr.* **23** 558